

Estimation of the periodic solutions of geometrically nonlinear structures by broadband excitation

*Original*

Estimation of the periodic solutions of geometrically nonlinear structures by broadband excitation / Anastasio, D.; Marchesiello, S.; Kerschen, G.. - ELETTRONICO. - (2024), pp. 2138-2150. ( ISMA - International Conference on Noise and Vibration Engineering Leuven (BEL) 9-11 September 2024).

*Availability:*

This version is available at: 11583/3005790 since: 2025-12-11T14:56:18Z

*Publisher:*

Katholieke Universiteit Leuven

*Published*

DOI:

*Terms of use:*

This article is made available under terms and conditions as specified in the corresponding bibliographic description in the repository

*Publisher copyright*

(Article begins on next page)

# Estimation of the periodic solutions of geometrically nonlinear structures by broadband excitation

D. Anastasio<sup>1</sup>, S. Marchesiello<sup>1</sup>, G. Kerschen<sup>2</sup>

<sup>1</sup> Politecnico di Torino, Department of Mechanical and Aerospace Engineering  
Corso Duca degli Abruzzi 24, 10129, Torino, Italy  
e-mail: [dario.anastasio@polito.it](mailto:dario.anastasio@polito.it)

<sup>2</sup> University of Liège, Aerospace and Mechanical Engineering Department  
Allée de la Découverte 9, 4000, Liège, Belgium

## Abstract

This paper proposes a methodology for indirectly estimating the periodic solutions of geometrically nonlinear structures using broadband excitation and nonlinear state-space modeling. The methodology is well-suited for thin-walled structures under large amplitude oscillations, and offers a valuable alternative to traditional harmonic-based methods, particularly in situations where such measurements are impractical or difficult to obtain. It relies first on the identification of the reduced-order nonlinear state-space model of the structure under broadband excitation, using the Modal-NSI (Nonlinear Subspace Identification) method. Then, the periodic solutions are studied by merging the Modal-NSI framework with the Harmonic Balance Method (HBM). A continuation technique is adopted to construct the Nonlinear Frequency Response Curves (NFRCs) of the structure, and a monodromy-based stability analysis is developed. The proposed methodology is validated on an experimental thin beam exhibiting a distributed geometrical nonlinearity.

## 1 Introduction

Understanding the behavior of geometrically nonlinear structures, particularly thin-walled and flexible elements, is crucial in various engineering applications. Generally, geometrical nonlinearity arises when a structure undergoes large-amplitude vibrations, resulting in a distributed nonlinear strain-displacement relation [1]. In the case of thin-walled structures, this creates a coupling between bending and in-plane stretching deformations, possibly resulting in hardening/softening effects and modal interactions. In this framework, a nonlinear model is very often obtained by projecting the physical domain onto a reduced-order basis, forming a reduced-order model [2]. Traditionally, investigating the periodic solutions of such systems relies on harmonic-based experimental measurements. Examples can be found in [3] and [4], where the experimental characterization of a geometrically nonlinear beam and a dieris-like structure undergoing large-amplitude vibrations is reported, respectively. Both cases fit a targeted nonlinear model structure to the Nonlinear Frequency Response Curves (NFRCs) of the considered system obtained from harmonic-based experimental measurements. This process is generally challenging and requires specific instrumentation, such as feedback control loops. This is needed since NFRCs are amplitude-response dependent, and several nonlinear phenomena may arise empirically, such as sub and super harmonics, bifurcations, unstable and isolated solutions, periodicity breaks or jumps. Feedback controls are therefore required for different reasons, such as keeping the solution on the desired branch and/or avoiding contaminations by higher harmonic contributions of the input excitation frequency. Several powerful approaches have been developed by the research community depending on the target of the identification and the controlled parameters [5-8].

An alternative approach that bypasses the need of control loops is to estimate first a valid nonlinear model for the considered system in an open-loop condition by using a broadband random excitation. Then, the

periodic solutions of the system can be studied based on the identified model. This approach has been successfully applied to estimate the nonlinear normal modes [9] and the NFRCs [10] of structures with localized nonlinearities. Both studies employed the Nonlinear Subspace Identification (NSI) technique to identify the state-space model from random measurements, in the frequency- and time- domains, respectively. Also, they both utilized a continuation technique to track the evolution of the solution over the selected control parameter, such as the pseudo-arch-length continuation [11]. The method presented in [10] in particular is referred to as HBM-NSI, as it incorporates a dedicated formulation of the Harmonic Balance Method (HBM) to study the periodic solutions within the nonlinear state-space framework of NSI. It is worth noting that such approach can deal with multiple modes simultaneously, since a broadband excitation is employed in the identification stage.

This paper presents a novel application of the HBM-NSI method for analyzing the periodic solutions of geometrically nonlinear structures. This approach tackles the limitations of traditional harmonic-based methods by utilizing the strengths of broadband random excitation and nonlinear state-space modeling. To account for the distributed nature of the nonlinearity, the state-space model is identified within a reduced-order domain, as detailed in [12].

The paper is organized as follows. Section 2 details the methodological approach. Section 3 presents the experimental application of a clamped thin beam structure. Section 4 presents a comparative analysis of the obtained results with system measurements across various modes and excitation levels. The results of the method will be compared with the system measurements for each considered case. Finally, Section 5 summarizes the key conclusions of the research.

## 2 Methods

This work proposes an indirect approach to estimate the periodic solutions of geometrically nonlinear structures. First, the nonlinear state-space model of the system is identified using broadband input-output data. The method used here to accomplish this task is detailed in [12], and produces a reduced-order state-space model using the linear normal modes (LNMs) of the structure as reduction basis. Subsequently, the methodology presented in [10] is applied in the reduced-order domain to estimate the periodic solutions of a nonlinear system in the NSI framework. This, in conjunction with the pseudo-arc-length continuation technique, allows to estimate the NFRCs of the system, and to investigate the stability of the obtained solutions.

### 2.1 Reduced-order nonlinear state-space formulation and identification

The equation of motion of a generic continuous system exhibiting a distributed nonlinear behavior can be written as:

$$M \left[ \frac{\partial^2}{\partial t^2} w(\mathbf{x}, t) \right] + C_v \left[ \frac{\partial}{\partial t} w(\mathbf{x}, t) \right] + K[w(\mathbf{x}, t)] = f(\mathbf{x}, t) - f^{\text{nl}}(w, \dot{w}), \quad \mathbf{x} \in \mathcal{D}, \quad (1)$$

where  $w(\mathbf{x}, t)$  is the displacement of the spatial coordinate  $\mathbf{x}$  in the domain  $\mathcal{D}$ ;  $M$  and  $K$  are the mass and stiffness linear differential operators [13],  $C_v$  is the proportional viscous damping operator, and  $f(\mathbf{x}, t)$  is the forcing input. The term  $f^{\text{nl}}(w, \dot{w})$  represents the nonlinear restoring force, i.e. the nonlinear part of the equation. It is put into the right-hand side so that it becomes a feedback to the underlying linear system (ULS) on the left-hand side and it is generally a function of both displacements  $w$  and velocities  $\dot{w}$ . For the case studied here, a distributed nonlinear behavior is considered and the LNMs  $\phi$  are used to operate in the reduced-order domain. Using the expansion theorem, the solution of eq. (1) can be expressed as:

$$w(\mathbf{x}, t) \cong \sum_{p=1}^P \phi_p(\mathbf{x}) \eta_p(t), \quad (2)$$

where  $\eta_p(t)$  is the  $p^{th}$  modal coordinate and a total of  $P$  LNMs are taken into account. This choice is very common when dealing with distributed nonlinearities due to its simplicity. However, it should be highlighted that LNMs do not decouple the equations of motion in a nonlinear setting. Applying the modal transformation expressed by eq. (2) to eq. (1) and under the assumption of self-adjoint operators, the following set of equations can be obtained:

$$m_r \ddot{\eta}_r + c_r \dot{\eta}_r + k_r \eta_r = q_r - q_r^{nl}, \quad r = 1, 2, \dots, P, \quad (3)$$

where  $m_r$ ,  $c_r$  and  $k_r$  are the modal mass, damping and stiffness respectively, and  $q_r(t) = \int_{\mathcal{D}} \phi_r(\mathbf{x}) f(\mathbf{x}, t) d\mathcal{D}$  is the modal force. The nonlinearity is now expressed by the term  $q_r^{nl}(t) = \int_{\mathcal{D}} \phi_r(\mathbf{x}) f^{nl}(\phi, \eta, \dot{\eta}) d\mathcal{D}$ . It is assumed hereafter that this term can be written as a linear-in-the-parameters basis function expansion up to a certain number  $J$ :

$$q_r^{nl} = \sum_{j=1}^J q_{j,r}^{nl} = \sum_{j=1}^J \Gamma_{j,r} b_{j,r}. \quad (4)$$

Each contribution  $q_{j,r}^{nl}$  contains an unknown coefficient  $\Gamma_{j,r}$  and a nonlinear basis function  $b_{j,r}$  that is supposed to be known. For structures exhibiting a geometrical nonlinearity, this likely results in a combination of modal coordinates coupling different vibration modes. The reader is referred to [12] for a detailed explanation.

If a state vector  $\boldsymbol{\lambda}_r = [\eta_r \quad \dot{\eta}_r]^T$  is defined, the nonlinear continuous state-space formulation can be retrieved:

$$\begin{cases} \dot{\boldsymbol{\lambda}}_r(t) = \mathbf{A}_r \boldsymbol{\lambda}_r(t) + \mathbf{B}_r^e \mathbf{q}_r^e(t) \\ \eta_r(t) = \mathbf{C}_r \boldsymbol{\lambda}_r(t) + \mathbf{D}_r^e \mathbf{q}_r^e(t) \end{cases} \quad (5)$$

where  $\mathbf{q}_r^e(t)$  is the extended modal input vector, defined as

$$\mathbf{q}_r^e(t) = [q_r(t) \quad b_{1,r}(t) \quad \dots \quad b_{J,r}(t)]^T \in \mathbb{R}^{(1+J) \times 1}. \quad (6)$$

The matrices  $\{\mathbf{A}, \mathbf{B}^e, \mathbf{C}, \mathbf{D}^e\}_r$  are the state, extended input, output and extended direct feedthrough matrices of the  $r^{th}$  mode. All the steps here presented will be related to the continuous-time formulation, but they can easily be adapted to the discrete one, for instance by applying the transformations reported in [14].

Also, eq. (5) represents in principle a single-degree-of-freedom system, as it is the result of the modal transformation. The model order in the state-space formulation is then theoretically  $N = 2$ . The quantities in eq. (5) have in this case the following dimensions:

$$\boldsymbol{\lambda}_r \in \mathbb{R}^{2 \times 1}, \quad \eta_r \in \mathbb{R}, \quad \mathbf{A}_r \in \mathbb{R}^{2 \times 2}, \quad \mathbf{B}_r^e \in \mathbb{R}^{2 \times (1+J)}, \quad \mathbf{C}_r \in \mathbb{R}^{1 \times 2}, \quad \mathbf{D}_r^e \in \mathbb{R}^{1 \times (1+J)}.$$

Subspace identification can be performed to identify the state-space matrices, rearranging the measured displacements into Hankel-type block matrices. The modal parameters and FRFs of the underlying linear system and the values of the coefficients of the nonlinear terms can be estimated by employing the NSI method. The reader is referred to [12] for further details.

If the steps described in eqs. (3)-(6) are repeated for each participating mode  $r$ , a set of  $P$  nonlinear modal state-space models  $\{\mathbf{A}, \mathbf{B}^e, \mathbf{C}, \mathbf{D}^e\}_{r=1, \dots, P}$  is obtained together with the full matrix of coefficients  $\boldsymbol{\Gamma}$ .

It is important to highlight that the knowledge of the LNMs is needed to build the reduced-order model. Note however that the LNMs must be computed just in the points where the sensors are located. Thus, a full analytical description of the mode shapes is not needed. LNMs are here estimated using a low-excitation level test (allegedly linear) with a linear identification algorithm. The nonlinear identification strategy to obtain the reduced-order state-space models is summarized in Figure 1.

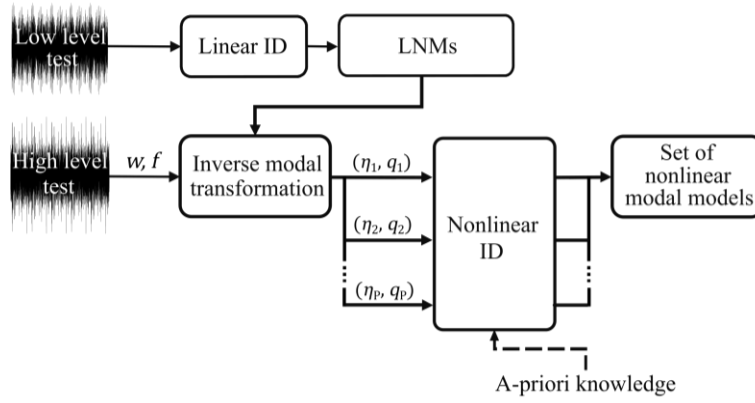


Figure 1: Flowchart of the reduced-order nonlinear system identification strategy.

## 2.2 Estimation of the periodic solutions, frequency curves and stability

It has been shown in [10] that the harmonic balance method can be directly applied to the nonlinear state-space formulation of NSI, such as the one in eq. (5). In particular, the extended force vector, the state vector and the system outputs can be represented as a Fourier series up to a selected order  $H$ . Taking the state vector as an example, this yields:

$$\lambda_r(t) = \mathbf{A}_r^{(0)} + \sum_{h=1}^H \left( \mathbf{A}_{C_r}^{(h)} \cos(h\omega t) + \mathbf{A}_{S_r}^{(h)} \sin(h\omega t) \right) = (\boldsymbol{\Theta}(t) \otimes \mathbf{I}_N) \mathbf{A}_r \quad (7)$$

where the Fourier coefficients are recast into the vector  $\mathbf{A}_r = [\mathbf{A}_r^{(0)\text{T}}, \mathbf{A}_{C_r}^{(1)\text{T}}, \mathbf{A}_{S_r}^{(1)\text{T}}, \dots, \mathbf{A}_{C_r}^{(H)\text{T}}, \mathbf{A}_{S_r}^{(H)\text{T}}]^\text{T}$ ,  $\mathbf{I}$  is the identity matrix,  $\otimes$  is the Kronecker tensor product and  $\boldsymbol{\Theta}(t)$  is equal to  $\boldsymbol{\Theta}(t) = [1 \ \cos(\omega t) \ \sin(\omega t) \ \dots \ \cos(H\omega t) \ \sin(H\omega t)]$ .

As commonly done in HB approaches, a Galerkin procedure can be applied to remove the time dependency. By introducing the operator  $\nabla$  defined as

$$\nabla = \text{diag}(\mathbf{0}, \quad \nabla_1, \quad \dots, \quad \nabla_H), \quad \nabla_h = h\omega \begin{bmatrix} 0 & 1 \\ -1 & 0 \end{bmatrix}, \quad (8)$$

the state-space equations are written in the frequency domain as follows (the detailed steps are reported in [10]):

$$\begin{cases} (\nabla \otimes \mathbf{I}_N) \mathbf{A}_r = (\mathbf{I}_{\tilde{H}} \otimes \mathbf{A}_c) \mathbf{A}_r + (\mathbf{I}_{\tilde{H}} \otimes \mathbf{B}_r^e) \mathbf{Q}_r^e \\ \mathbf{I}_{\tilde{H}} \mathbf{H}_r = (\mathbf{I}_{\tilde{H}} \otimes \mathbf{C}_r) \mathbf{A}_r + (\mathbf{I}_{\tilde{H}} \otimes \mathbf{D}_r^e) \mathbf{Q}_r^e \end{cases}, \quad (9)$$

where  $\tilde{H} = 2H + 1$ , and the vectors  $\mathbf{Q}_r^e$  and  $\mathbf{H}_r$  contain the Fourier coefficients of  $\mathbf{q}_r^e(t)$  and  $\eta_r(t)$ , similarly to eq. (7). The input-output relation can be re-written by manipulating eq. (9) as:

$$\mathbf{I}_{\tilde{H}} \mathbf{H}_r = \mathbf{T}_r(\omega) \mathbf{Q}_r^e, \quad \mathbf{T}_r = (\mathbf{I}_{\tilde{H}} \otimes \mathbf{D}_r^e) + (\mathbf{I}_{\tilde{H}} \otimes \mathbf{C}_r) (\nabla \otimes \mathbf{I}_N - \mathbf{I}_{\tilde{H}} \otimes \mathbf{A}_c)^{-1} (\mathbf{I}_{\tilde{H}} \otimes \mathbf{B}_r^e). \quad (10)$$

The matrix  $\mathbf{T}_r(\omega)$  relates the inputs to the outputs and is a function of the identified state-space matrices. The vector  $\mathbf{Q}_r^e$  of the  $r^{\text{th}}$  mode contains the Fourier coefficients of both the modal forcing term and the nonlinear basis functions. These depend on modal displacements and/or velocities, and therefore their Fourier coefficients are generally a function of  $\mathbf{H}_1, \dots, \mathbf{H}_p$ . Since the vector  $\mathbf{H}_r$  of the  $r^{\text{th}}$  mode is unknown, a recursive methodology must be implemented to solve eq. (10). In particular, the following nonlinear problem can be deduced:

$$\boldsymbol{\varepsilon}_r(\mathbf{H}_r, \omega) = \mathbf{T}_r(\omega) \mathbf{Q}_r^e - \mathbf{I}_{\tilde{H}} \mathbf{H}_r = \mathbf{0}, \quad (11)$$

which can be solved for all the participating modes using an incremental-iterative Newton-Raphson procedure. An efficient way to compute the quantity  $\mathbf{Q}_r^e$  is to apply the alternating frequency/time domain technique (AFT) [15]. It consists in using the inverse Fourier transform to compute the nonlinear basis functions and thus the extended (modal) forces in the time domain. The vector  $\mathbf{Q}_r^e$  can then be obtained by switching back to the frequency domain as:

$$\begin{array}{ccc} \mathbf{H}_1 & \xrightarrow{\text{FFT}^{-1}} & \eta_1(t) \\ \vdots & & \vdots \\ \mathbf{H}_P & \xrightarrow{\text{FFT}^{-1}} & \eta_P(t) \end{array} \rightarrow \begin{array}{c} \mathbf{q}_1^e(t) = [q_1, b_{1,1}, \dots, b_{J,1}]^T \\ \vdots \\ \mathbf{q}_P^e(t) = [q_P, b_{1,P}, \dots, b_{J,P}]^T \end{array} \xrightarrow{\text{FFT}} \begin{array}{c} \mathbf{Q}_1^e(\mathbf{H}_1, \dots, \mathbf{H}_P) \\ \vdots \\ \mathbf{Q}_P^e(\mathbf{H}_1, \dots, \mathbf{H}_P) \end{array}. \quad (12)$$

When eq. (11) is solved in conjunction with a continuation technique, the frequency response curve over a certain range of frequencies can be obtained. The stability of the periodic solutions over the NFRC can be studied as well, by employing several techniques [16]. In this work, the monodromy-based approach presented in [10] is adopted, since its formulation is coherent with the state-space model structure of NSI. The Floquet multipliers are therefore estimated at each  $\omega$ , represented in the complex plane and compared with the unit circle. In particular [17]:

- a fold bifurcation is detected when a Floquet multiplier crosses the real axis through  $+1$ ;
- a Neimark-Sacker bifurcation is detected when two complex-conjugate multipliers cross the unit circle;
- a period doubling bifurcation is detected when one Floquet multiplier crosses the real axis through  $-1$ .

Once the *modal* output  $\mathbf{H}_r(\omega)$  has been computed for each frequency and each mode, the direct modal transformation can be applied by using again the estimated LNMs to obtain the *physical* output responses in the sensors locations  $\mathbf{W}(\omega)$ .

It is important to highlight that the accuracy of the predicted periodic solutions strongly depends on the data used for the estimation of the nonlinear state-space model. In particular, the range of motion (ROM) of the periodic solutions should be largely within the one covered by the broadband data to avoid extrapolation issues, as outlined in [10], [18].

### 3 Experimental application

The experimental application consists of a clamped thin steel beam of thickness 0.75 mm, instrumented with accelerometers and excited with a shaker. The system has already been presented in [12], where the nonlinear identification of the reduced-order state-space models has been conducted employing broadband measurements over the first three bending modes. A total of 8 accelerometers are used, plus a load cell on the head of the shaker to record the input. The position of the sensors is summarized in Table 1, while a photo of the setup is shown in Figure 2.

Table 1: Position of the sensors and type.

Sensor #	1	2	3	4	5	6	7	8
	Impedance head	Accelerometers						
Distance from the right end (mm)	15	35	105	175	245	315	385	455

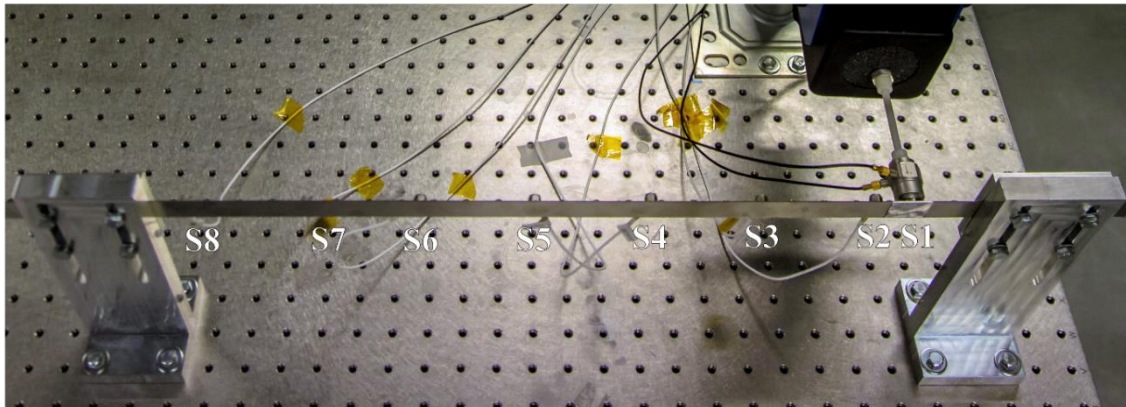


Figure 2: Photo of the experimental test rig.

### 3.1 Previous findings

Multisine excitations with random phase have been used to characterize the nonlinearity and estimate the model parameters. The frequency range of the forcing input was 14 Hz to 100 Hz and the sampling frequency 6400 Hz. Two excitation levels were considered: low (0.01 V RMS) and high (0.07 V RMS), which resulted in the ROMs depicted in Figure 3 on the sensors location. The displacements values have been obtained by double integration of the accelerometers signals.

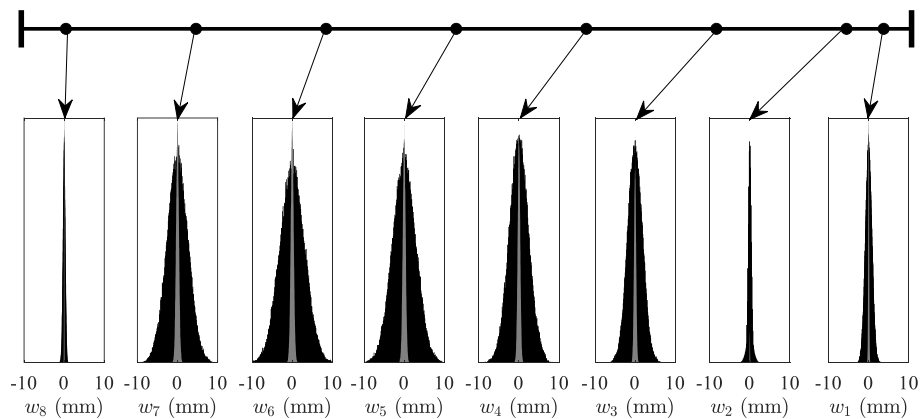


Figure 3: Histograms of the measured displacements, multisine excitations. Gray: low excitation level; black: high excitation level.

The experimental frequency response function (FRF) related to the 2<sup>nd</sup> sensor is reported in Figure 4 together with the noise and the total distortion estimations, for two excitation levels.

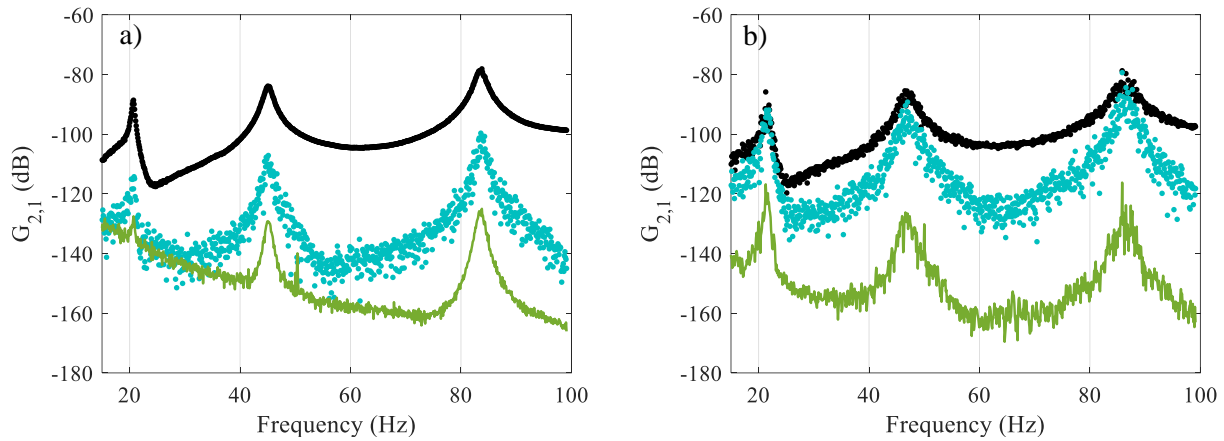


Figure 4: Experimental FRF (receptance) related to sensor 2 in dB scales. a) Low-level (linear); b) High-level. Black line: FRF; green line: disturbance noise level; light blue dots: total distortions level.

Following the flowchart of Figure 1, the low excitation level was first considered to estimate the LNMs of the structure and the modal parameters of the underlying linear system. This was accomplished by using a linear subspace identification technique, with the stabilization diagram reported in Figure 5. Three modes clearly stabilize and correspond to the first three bending modes of the structure. The estimated modal parameters are listed in Table 2 and the corresponding LNMs are used as reduction basis for the nonlinear system identification stage.

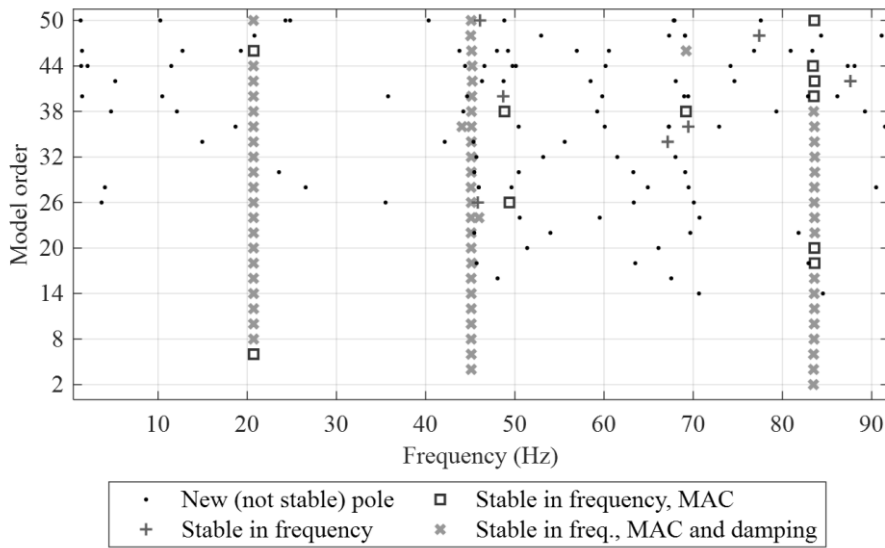


Figure 5: Stabilization diagram, low-level. Stabilization thresholds for natural frequency, damping ratio and MAC are 0.5%, 10% and 99.5%, respectively.

The high-level measurement was employed for the nonlinear system identification in the *modal* domain. The vector of nonlinear basis functions used in the NSI method was in this case:

$$\begin{aligned}
 \mathbf{b}^{nl} &= -\text{vec}\{\eta_j^m \eta_r^p\} = -[\eta_1^2, \eta_1^3, \eta_1^3, \eta_2 \eta_1, \eta_2^2 \eta_1, \eta_2 \eta_1^2, \dots, \eta_3^3]^T, \\
 j &= 1, \dots, 3, \quad r = 1, \dots, 3, \quad m = 1, 2, \quad p = 1, 2.
 \end{aligned}
 \tag{13}$$

The reader is referred to [12] for more insights on this choice. The stabilization diagrams of the three underlying linear systems are plotted in Figure 6, while the corresponding modal parameters are listed in Table 2 and compared to the linear results.

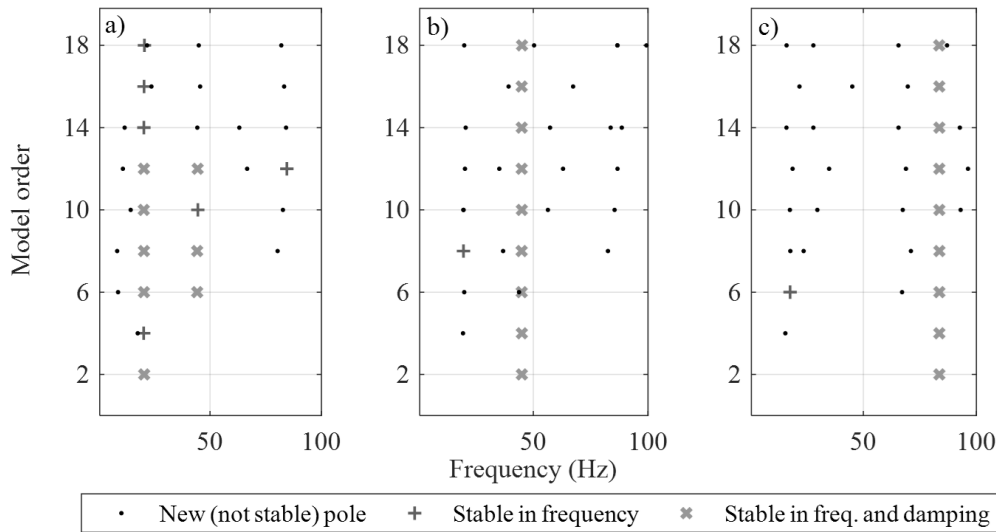


Figure 6: Stabilization diagrams of the modal ULSs, high-level. Stabilization thresholds for natural frequency and damping ratio are 0.5%, 10%, respectively. a) Mode number 1; b) Mode number 2; c) Mode number 3.

Table 2: Summary of the identified modal parameters of the ULS with linear and nonlinear identification methods.

Mode number	Frequency (Hz)		Damping ratio (%)	
	Linear ID. (low-level)	Nonlinear ID. (high-level, ULS)	Linear ID. (low-level)	Nonlinear ID. (high-level, ULS)
1	20.7	20.5	1.2	1.2
2	45.1	45.1	1.7	2.2
3	83.6	83.8	1.1	2.0

A validation data set was also used in [12] to quantify the residuals over the outputs of the system. Results showed a very good level of accuracy in predicting the behavior of the system under random excitation with (nonlinear) large-amplitude oscillations, with relative RMS error of approximately 6%. The identified nonlinear model will be used in the Section 4 for the estimation of the periodic solutions and the NFRCs.

### 3.2 Frequency-sweep tests

A series of frequency-sweep tests has been conducted on the structure and will be used to validate the estimated frequency response curves obtained using the proposed methodology. The tests, listed in Table 3, investigate the first and second modes of the structure under varying excitation levels. As an example, Figure 7 illustrates the acceleration measured by the 3<sup>rd</sup> sensor during three different tests. A noticeable hardening effect with a jump phenomenon is visible in Figure 7 (a) and (c) around the first and second resonances, respectively.

Table 3: Frequency-sweep tests.

Test nr.	Targeted mode	Level (V)	Min. freq. (Hz)	Max. freq. (Hz)	Rate (Hz/s)	Direction
1	1	0.03	18	25	0.2	up, down
2	2	0.01	40	50	0.2	up, down
3	2	0.05	40	50	0.2	up, down

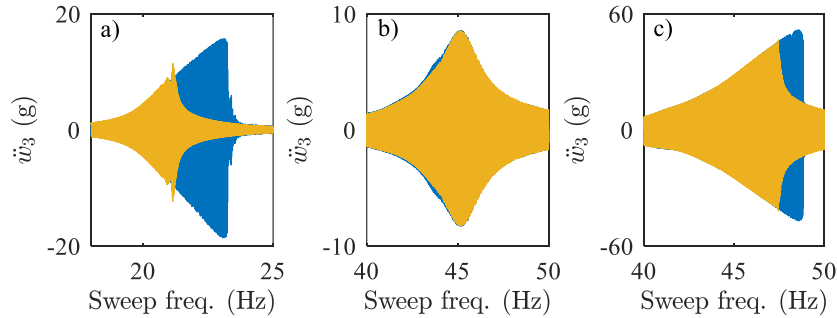


Figure 7: Acceleration of sensor 3 for the sweep-up (blue) and down (yellow) tests. a) Test nr. 1; b) Test nr. 2; c) Test nr. 3.

## 4 Results and discussions

The proposed methodology is applied to the considered structure to estimate the NFRCs across the first two modes of vibration and using the nonlinear reduced-order state-space model estimated in Section 2. It is worth reminding that the identification is performed just once by using a broadband measurement encompassing all the relevant modes. Once the state-space parameters of eq. (5) are estimated using the technique outlined in Section 2.2, the periodic solutions of the system can be readily analyzed.

To facilitate a direct comparison with experiments, three simulations are conducted under the same conditions specified in Table 3. The estimated NFRCs are calculated considering  $H = 9$  harmonics and then compared with the experimental results of both up and down frequency sweeps.

The *physical* displacements  $\mathbf{W}(\omega)$  will be considered in the following. They are computed by projecting the modal outputs, obtained by solving the nonlinear problem of eq. (11), back to the physical domain using eq. (2).

### 4.1 Test 1: targeted mode 1, 0.03 V

This section focuses on the frequency sweep around the first mode of vibration. The estimated NFRCs in correspondence of 4<sup>th</sup> and 6<sup>th</sup> sensors are plotted in Figure 8 (a) and (b), respectively. A fold bifurcation (FB) can be observed, followed by an unstable solution branch. This behavior aligns well with the experimental observations from both up and down frequency sweeps, and the model accurately predicts the jumping frequency. However, a minor discrepancy exists between the predicted lower stable solution and the experimental sweep-down response in the range of 21-23 Hz. Similar results are observed for the responses of other sensors.

Figure 9 illustrates the contributions of individual harmonics to the predicted response of the 4<sup>th</sup> sensor. The first harmonic  $|W_4^{(1)}|$  dominates the response, and accounts for roughly 96% of the response in correspondence of the jumping frequency. At this frequency, it is followed by third (2%), second (1%), fourth (0.4%) and fifth (0.3%) harmonics. The other harmonics are negligible in the entire frequency range.

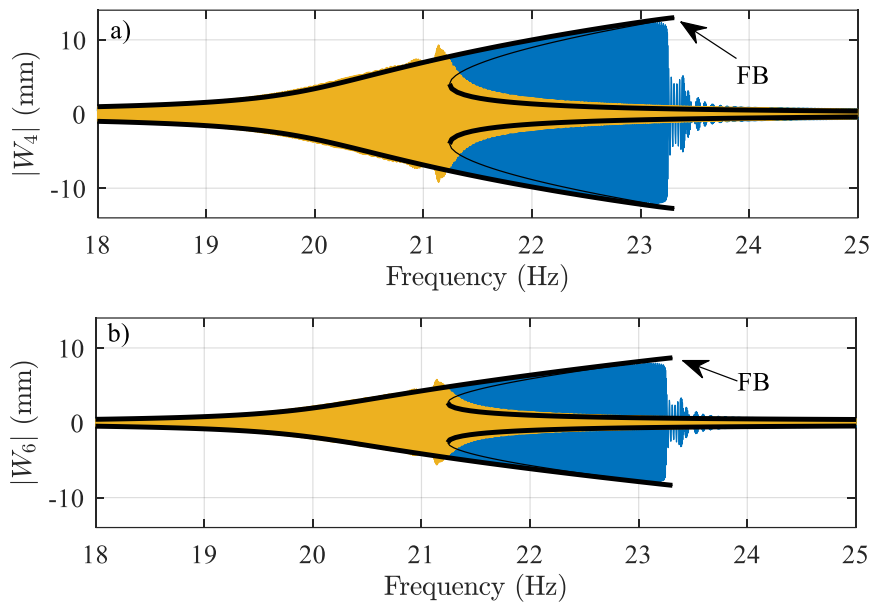


Figure 8: Frequency response, test 1. a) Sensor 4; b) Sensor 6. Blue line: experimental sweep-up; yellow-line: experimental sweep-down; black line: HBM-NSI result. The unstable branch is depicted with a thin line.

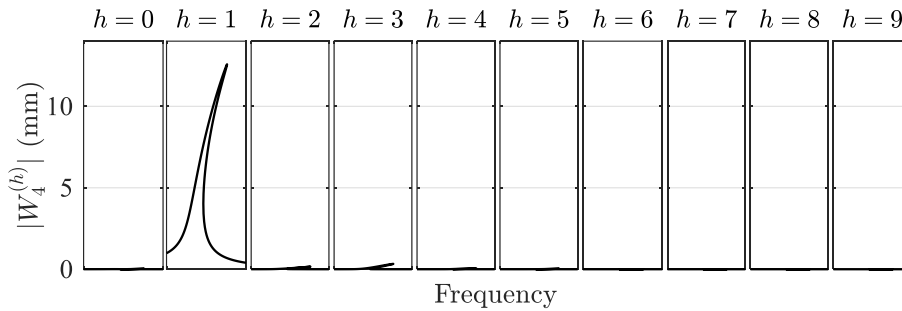


Figure 9: Single harmonic contributions on the selected frequency range, test 1, sensor 4.

### 4.2 Test 2: targeted mode 2, 0.01 V

This section and the following one focus on the frequency sweep around the second mode of vibration. Here, the excitation level is the lowest measured, resulting in an almost linear response. This can be observed in the estimated frequency response curve and the corresponding harmonic contributions of Figure 10 (for sensor nr. 7). The comparison with the experimental data reveals a satisfying accuracy also in this case. This confirms the ability of the estimated model to capture the underlying linear dynamics of the actual system at low excitation levels. Similar results are observed for the responses of other sensors.

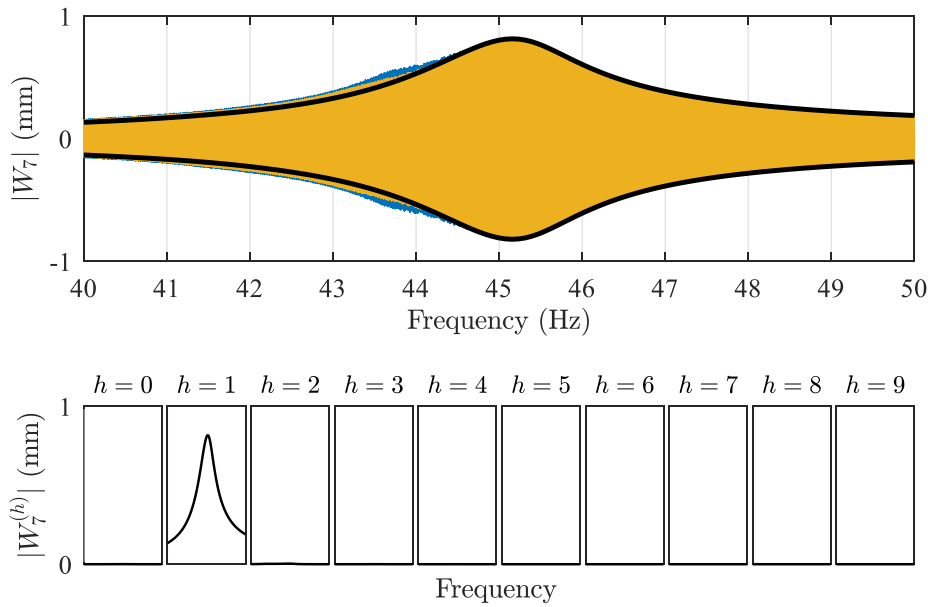


Figure 10: Frequency response, test 2, sensor 7. Blue line: experimental sweep-up; yellow-line: experimental sweep-down; black line: HBM-NSI result. The single harmonic contributions are also displayed on the same frequency range.

### 4.3 Test 3: targeted mode 2, 0.05 V

The highest excitation level around the second mode is considered in this section. Figure 11 shows the estimated NFRC for the 3<sup>rd</sup> sensor, exhibiting a fold bifurcation (FB) followed by an unstable solution branch.

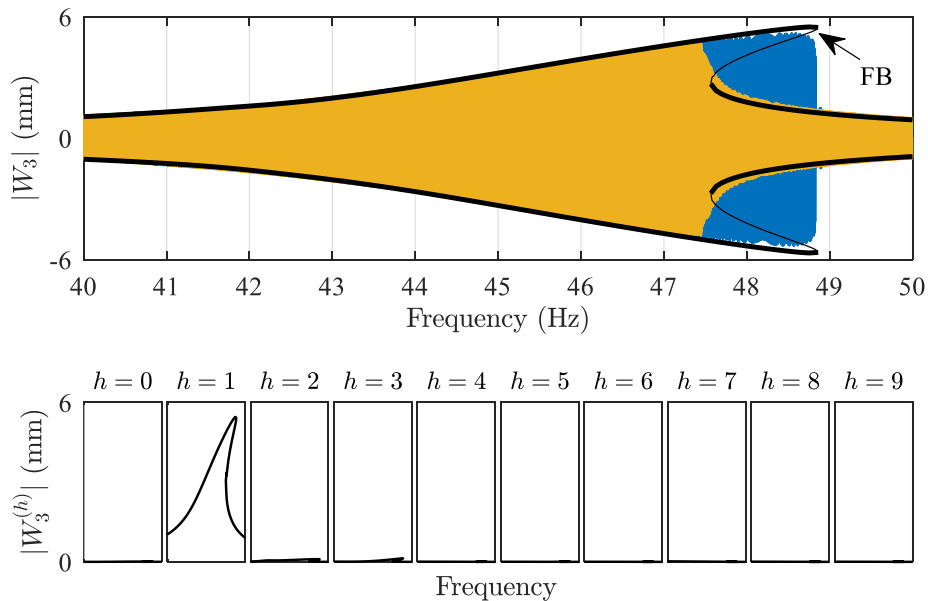


Figure 11: Frequency response, test 3, sensor 3. Blue line: experimental sweep-up; yellow-line: experimental sweep-down; black line: HBM-NSI result (unstable branch with thin line). The single harmonic contributions are also displayed on the same frequency range.

This is coherent with the experimental observations of up and down sweeps displayed in blue and yellow, respectively. The model accurately predicts the jumping frequency in this case as well. In terms of the harmonic content of the response, the results are quite similar to those observed in test 1. The first harmonic remains dominant, accounting for approximately 97% of the system response in correspondence of the jumping frequency. This trend is consistent across the responses measured by other sensors.

## 5 Conclusions

This work presented a methodology for indirectly estimating the periodic solutions of geometrically nonlinear structures using broadband excitation and nonlinear state-space modeling. The method relies first on the experimental identification of the reduced-order nonlinear state-space model of the structure under broadband excitation. The linear normal modes have been used in this paper as a projection space, combined with the nonlinear subspace identification (NSI) technique. An ad-hoc formulation of the harmonic balance method was then derived within the reduced-order NSI framework, to study the periodic solutions of the system and estimate the frequency response curves. The stability of the solutions is further assessed using a monodromy-based approach.

The proposed methodology was validated on an experimental thin beam exhibiting large-amplitude oscillations and distributed geometrical nonlinearity. The nonlinear state-space model was initially estimated considering a multisine excitation with random phase. Subsequently, the proposed methodology was adopted to estimate the nonlinear frequency response curves and analyze the stability of the solutions. The results were compared with experimental frequency sweeps around the first and second bending modes with various excitation levels.

The validation test demonstrated the effectiveness of the identification strategy in predicting periodic solutions without requiring harmonic-based experimental measurements. Notably, a single high-level broadband measurement suffices to estimate the behavior of the periodic solutions of the system across multiple vibration modes, with a satisfying accuracy. The indirect estimation approach offers therefore a valuable alternative to traditional harmonic-based methods, particularly in situations where such measurements are impractical or difficult to obtain.

## References

- [1] A. H. Nayfeh and P. F. Pai, *Linear and nonlinear structural mechanics*, vol. 40, no. 2. 2004. doi: 10.1007/s11012-005-0327-y.
- [2] C. Touzé, O. Thomas, and A. Huberdeau, “Asymptotic non-linear normal modes for large-amplitude vibrations of continuous structures,” *Comput. Struct.*, vol. 82, no. 31–32, pp. 2671–2682, 2004, doi: 10.1016/j.compstruc.2004.09.003.
- [3] M. Claeys, J. J. Sinou, J. P. Lambelin, and B. Alcoverro, “Multi-harmonic measurements and numerical simulations of nonlinear vibrations of a beam with non-ideal boundary conditions,” *Commun. Nonlinear Sci. Numer. Simul.*, vol. 19, no. 12, pp. 4196–4212, 2014, doi: 10.1016/j.cnsns.2014.04.008.
- [4] X. Wang, T. L. Hill, and S. A. Neild, “Frequency response expansion strategy for nonlinear structures,” *Mech. Syst. Signal Process.*, vol. 116, pp. 505–529, 2019, doi: 10.1016/j.ymssp.2018.06.027.
- [5] L. Renson, A. Gonzalez-Buelga, D. A. W. Barton, and S. A. Neild, “Robust identification of backbone curves using control-based continuation,” *J. Sound Vib.*, vol. 367, pp. 145–158, 2016, doi: 10.1016/j.jsv.2015.12.035.

- [6] S. Peter and R. I. Leine, "Excitation power quantities in phase resonance testing of nonlinear systems with phase-locked-loop excitation," *Mech. Syst. Signal Process.*, vol. 96, pp. 139–158, 2017, doi: 10.1016/j.ymsp.2017.04.011.
- [7] T. Karaağaçlı and H. N. Özgüven, "Experimental modal analysis of nonlinear systems by using response-controlled stepped-sine testing," *Mech. Syst. Signal Process.*, vol. 146, 2021, doi: 10.1016/j.ymsp.2020.107023.
- [8] J. Taghipour et al., "Harmonic-Balance-Based parameter estimation of nonlinear structures in the presence of Multi-Harmonic response and force," *Mech. Syst. Signal Process.*, vol. 162, 2022, doi: 10.1016/j.ymsp.2021.108057.
- [9] J. P. Noël, L. Renson, C. Grappasonni, and G. Kerschen, "Identification of nonlinear normal modes of engineering structures under broadband forcing," *Mech. Syst. Signal Process.*, vol. 74, pp. 95–110, 2016, doi: 10.1016/j.ymsp.2015.04.016.
- [10] D. Anastasio and S. Marchesiello, "Nonlinear frequency response curves estimation and stability analysis of randomly excited systems in the subspace framework," *Nonlinear Dyn.*, 2023, doi: 10.1007/s11071-023-08280-6.
- [11] L. Xie, S. Baguet, B. Prabel, and R. Dufour, "Bifurcation tracking by Harmonic Balance Method for performance tuning of nonlinear dynamical systems," *Mech. Syst. Signal Process.*, vol. 88, pp. 445–461, 2017, doi: 10.1016/j.ymsp.2016.09.037.
- [12] D. Anastasio, S. Marchesiello, G. Kerschen, and J. P. Noël, "Experimental identification of distributed nonlinearities in the modal domain," *J. Sound Vib.*, vol. 458, pp. 426–444, 2019, doi: 10.1016/j.jsv.2019.07.005.
- [13] L. Meirovitch, *Principles and techniques of vibrations*. Upper Saddle River, N.J: Prentice Hall, 1997.
- [14] E. Reynders and G. De Roeck, "Reference-based combined deterministic–stochastic subspace identification for experimental and operational modal analysis," *Mech. Syst. Signal Process.*, vol. 22, pp. 617–637, 2008, doi: 10.1016/j.ymsp.2007.09.004.
- [15] T. M. Cameron and J. H. Griffin, "An Alternating Frequency/Time Domain Method for Calculating the Steady-State Response of Nonlinear Dynamic Systems," *J. Appl. Mech.*, vol. 56, no. 1, pp. 149–154, 1989, doi: 10.1115/1.3176036.
- [16] L. Peletan et al., "A comparison of stability computational methods for periodic solution of nonlinear problems with application to rotordynamics," *Nonlinear Dyn.*, vol. 72, pp. 671–682, 2013, doi: 10.1007/s11071-012-0744-0.
- [17] G. R. Itovich and J. L. Moiola, "On period doubling bifurcations of cycles and the harmonic balance method," *Chaos Solitons Fractals*, vol. 27, no. 3, pp. 647–665, 2006, doi: 10.1016/J.CHAOS.2005.04.061.
- [18] M. Schussler and O. Nelles, "Extrapolation behavior comparison of nonlinear state space models," *IFAC-PapersOnLine*, vol. 54, pp. 487–492, 2021, doi: 10.1016/j.ifacol.2021.08.407.